Clim Dyn
DOI 10.1007/s00382-014-2385-0

Peak-summer East Asian rainfall predictability and prediction part I: Southeast Asia

Wen Xing · Bin Wang · So-Young Yim

Received: 26 May 2014 / Accepted: 14 October 2014

Abstract The interannual variation of East Asia summer monsoon (EASM) rainfall exhibits considerable differences between early summer [May–June (MJ)] and peak summer [July–August (JA)]. The present study focuses on peak summer. During JA, the mean ridge line of the western Pacific subtropical High (WPSH) divides EASM domain into two sub-domains: the tropical EA (5°N–26.5°N) and subtropical-extratropical EA (26.5°N–50°N). Since the major variability patterns in the two sub-domains and their origins are substantially different, the Part I of this study concentrates on the tropical EA or Southeast Asia (SEA). We apply the predictable mode analysis approach to explore the predictability and prediction of the SEA peak summer rainfall. Four principal modes of interannual rainfall variability during 1979–2013 are identified by EOF analysis: (1) the WPSH-dipole sea surface temperature (SST) feedback mode in the Northern Indo-western Pacific warm pool associated with the decay of eastern Pacific El Niño/Southern Oscillation (ENSO), (2) the central Pacific-ENSO mode, (3) the Maritime continent SST-Australian High coupled mode, which is sustained by a positive feedback between anomalous Australian high and sea surface temperature anomalies (SSTA) over Indian Ocean, and (4) the ENSO developing mode. Based on understanding of the sources of the predictability for each mode, a set of physics-based empirical (P-E) models is established for prediction of the first four leading principal components (PCs). All predictors are selected from either persistent atmospheric lower boundary anomalies from March to June or the tendency from spring to early summer. We show that these four modes can be predicted reasonably well by the P-E models, thus they are identified as the predictable modes. Using the predicted PCs and the corresponding observed spatial patterns, we have made a 35-year cross-validated hindcast, setting up a bench mark for dynamic models' predictions. The P-E hindcast prediction skill represented by domain-averaged temporal correlation coefficient is 0.44, which is twice higher than the skill of the current dynamical hindcast, suggesting that the dynamical models have large rooms to improve. The maximum potential attainable prediction skills for the peak summer SEA rainfall is also estimated and discussed by using the PMA. High predictability regions are found over several climatological rainfall centers like Indo-China peninsula, southern coast of China, southeastern SCS, and Philippine Sea.

Keywords East Asian monsoon · Monsoon rainfall prediction · Physical-empirical model · Monsoon predictability · Predictable mode analysis

W. Xing
Physical Oceanography Laboratory/Qingdao Collaborative Innovation Center of Marine Science and Technology, Ocean University of China, Qingdao 266100, China

W. Xing · B. Wang
International Pacific Research Center and Department of Meteorology, University of Hawaii at Manoa, Honolulu, HI 96822, USA

B. Wang
Earth System Modeling Center, Nanjing University of Information Science and Technology, Nanjing 210044, China

S.-Y. Yim (✉)
Korea Meteorological Administration, Seoul 156-720, Korea
e-mail: hiyim03@gmail.com

1 Introduction

The East Asia summer monsoon (EASM) is a distinctive component of the Asian monsoon system due to unique

Published online: 19 November 2014

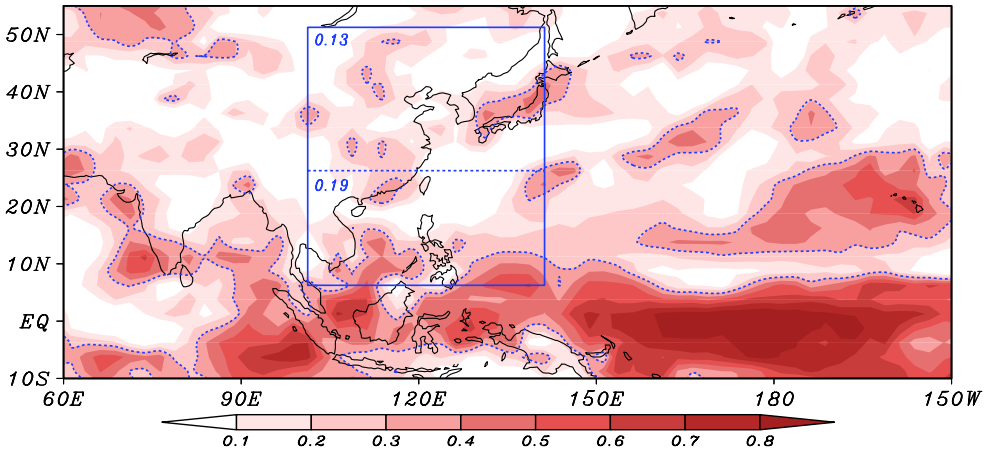

Fig. 1 The temporal correlation coefficient (TCC) skill for JA precipitation prediction using the *four* coupled models' multi-model ensemble (MME) initiated from the first day of July for the 32 years of 1979–2010. The *dashed contour* is the TCC skill of 0.30 with statistically significance at 90 % confidence level. *Blue box* indicates the EASM region used in this study (100°E–140°E, 5°N–50°N) and the number in the *upper-left* corner of each *blue box* is the averaged TCC skill over that region. The averaged TCC over the whole EASM region is 0.16

orographic forcing and huge thermal contrasts between Asian continent and Pacific Ocean (Chen and Chang 1980; Tao and Chen 1987; Lau et al. 1988; Ding 1992; Wang et al. 2001). The seasonal rainfall exhibits significant variability at interannual time scale (Kosaka and Yang 1997; Chang et al. 2000; Wang et al. 2000; Ding and Chan 2005). The great impact of monsoon-related droughts and floods on the dense population of East Asia (EA) has motivated many climate scientists to investigate the causes and predictability of EASM rainfall variations.

It has been recognized that the El Niño/Southern Oscillation (ENSO), spring North Atlantic Oscillation (NAO), and Eurasian or Tibetan snow cover can exert effects on the EASM (e.g. Wang et al. 2000, 2008; Liu and Yanai 2002; Zhang et al. 2004; He et al. 2007; Wu et al. 2009). Wu et al. (2009) established an empirical model to predict the EASM strength by combination of ENSO and spring NAO. Fan et al. (2012) developed two statistical prediction schemes including the interannual increment approach to improve the seasonal prediction of the EASM's strength. The predictability of EASM is studied from the reproduction of land-sea thermal contrast changes (Zhou and Zou 2010). These works all dealt with June–July–August mean anomalies as most studies did in the past. Note however, the EASM has its own indigenous monsoon calendar (LinHo and Wang 2002). Over India, the rainy season includes June through September, but over East Asian land areas the rainy season start from May and largely terminates at the end of August (Wang and LinHo 2002).

Recently, a new strategy was suggested for prediction of EASM, i.e., to predict early summer [May–June (MJ)] and peak summer [July–August (JA)] rainfall anomalies separately. This strategy was based on the following consideration: (a) there are remarkable differences in the mean state of precipitation and circulation, and (b) the principal modes of interannual precipitation variability have distinct structures during MJ and JA (Wang et al. 2009; Li and Zhou 2011; Qin et al. 2013). Recently, the early summer EA rainfall predictability has been investigated. This study takes peak-summer (JA) precipitation variability as the target.

Dynamical prediction of peak summer rainfall over EA remains a great challenge (Wang et al. 2005; Wu and Li 2008). Figure 1 shows the temporal correlation coefficient (TCC) for JA precipitation prediction at each grid using four state-of-the-art climate models' multi-model ensemble (MME). As can be seen, the area-averaged TCC over the EASM region (100°E–140°E, 5°N–50°N) is only 0.16 during 1979–2010 with higher skill over the tropical EA (0.19) and lower skill over the northern EA (0.13). The prediction skill that is significant at 90 % confidence level only occurs over the southern South China Sea (SCS), a small part of Philippine Sea and north of Japan. The predictability of MME for JA precipitation over most EASM region remains very limited. Considering the poor prediction skill of dynamical models, one would wonder to what extent the peak-summer EASM rainfall is predictable.

Since the EASM is a compound system that encompasses tropical and subtropical systems and cold air activities over the mid- and high-latitudes (Zhu et al. 1986), it is difficult to identify the physical processes determining the rainfall variability in the entire EASM region (100°E–140°E, 5°N–50°N). As shown in Fig. 2, there are two rainfall maxima over EA during JA. One is located at the tropical monsoon trough region centered on the Philippine Sea and eastern SCS, and

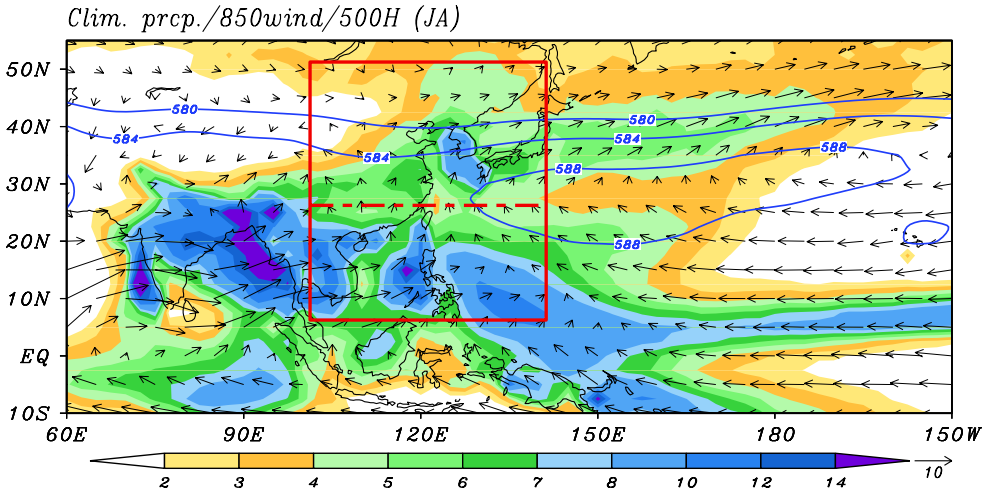

Fig. 2 Climatological mean precipitation rate (*color shading* in units of mm day^{-1}), 850-hPa winds (*arrows* in units of m s^{-1}), and 500-hPa geopotential height (*contours* in units of 10 gpm) averaged for July–August (JA) from 1979 to 2013. The *red solid box* indicates the EASM region used in this study (100°E–140°E, 5°N–50°N). The *red dashed line* is the ridge line of the western Pacific subtropical high, which divides the EASM domain into SEA (100°E–140°E, 5°N–26.5°N) and NEA (100°E–140°E, 26.5°N–50°N)

the other is over the vicinity of Korea peninsula. The two maximum rainfall regions are separated by a minimum zone along the ridge line of the western Pacific subtropical high (WPSH) around 26°N–27°N. Thus, we divide EASM region into tropical EA or Southeast Asia (SEA, 100°E–140°E, 5°N–26.5°N) and subtropical–extratropical EA or northern EA (NEA, 100°E–140°E, 26.5°N–50°N). The rainfall variability of EASM during the peak summer will be presented for SEA and NEA separately in the Part I and Part II of this series of paper, respectively.

The Part I of this paper aims at understanding the controlling factors of the variability and estimating the predictability of the peak-summer rainfall in the SEA. Section 2 briefly describes the datasets, models and methodology used in this study. Section 3 presents principle modes of JA precipitation variability over SEA and explores physical processes governing each principal mode. In Sect. 4 we establish physical-based empirical (P-E) model to estimate the extent to which we can predict these dominant modes. Section 5 summarizes major conclusions.

2 Data and method

2.1 Data

The data used in this study comprise monthly mean precipitation from Global Precipitation Climatology Project (GPCP, v2.2) datasets (Huffman et al. 2011), monthly mean sea surface temperature (SST) from NOAA Extended Reconstructed SST (ERSST, v3b) (Smith et al. 2008), and the monthly mean circulation data from the newly released ERA interim (Dee et al. 2011). The data period chosen in this study is from 1979 to 2013. Peak-summer rainfall anomalies are calculated by the deviation of JA mean rainfall from the 35-year climatology (1979–2013).

Four state-of-the-art atmosphere–ocean–land coupled models are also used in this study, including (1) NCEP (National Center for Environmental Prediction) CFS version 2 (Saha et al. 2013), (2) ABOM (Australia Bureau of Meteorology) POAMA version 2.4 (Hudson et al. 2010), (3) GFDL (Geophysical Fluid Dynamics Laboratory) CM version 2.1 (Delworth et al. 2006), and (4) FRCGC (Frontier Research Center for Global Change) SINTEX-F model (Luo et al. 2005). The four coupled models which are available from 1979 to 2010 are all with early July initial conditions. The MME prediction was made by simply averaging four coupled models' ensemble mean anomalies after removing their own climatology.

2.2 Method

The predictable mode analysis (PMA) is applied to establish P-E prediction models and to estimate potential predictability. The detailed methodology is described by Wang et al. (2007, 2014). Empirical orthogonal function (EOF) analysis of the JA mean precipitation anomalies from 1979 to 2013 is first performed to extract several leading principle modes of SEA rainfall variability.

We focus on the first four modes because when we use two precipitation datasets (GPCP and CMAP), these modes show similar spatial patterns and principal components (PCs) while the higher modes are different, which means that the higher modes tend to be noisy and uncertain

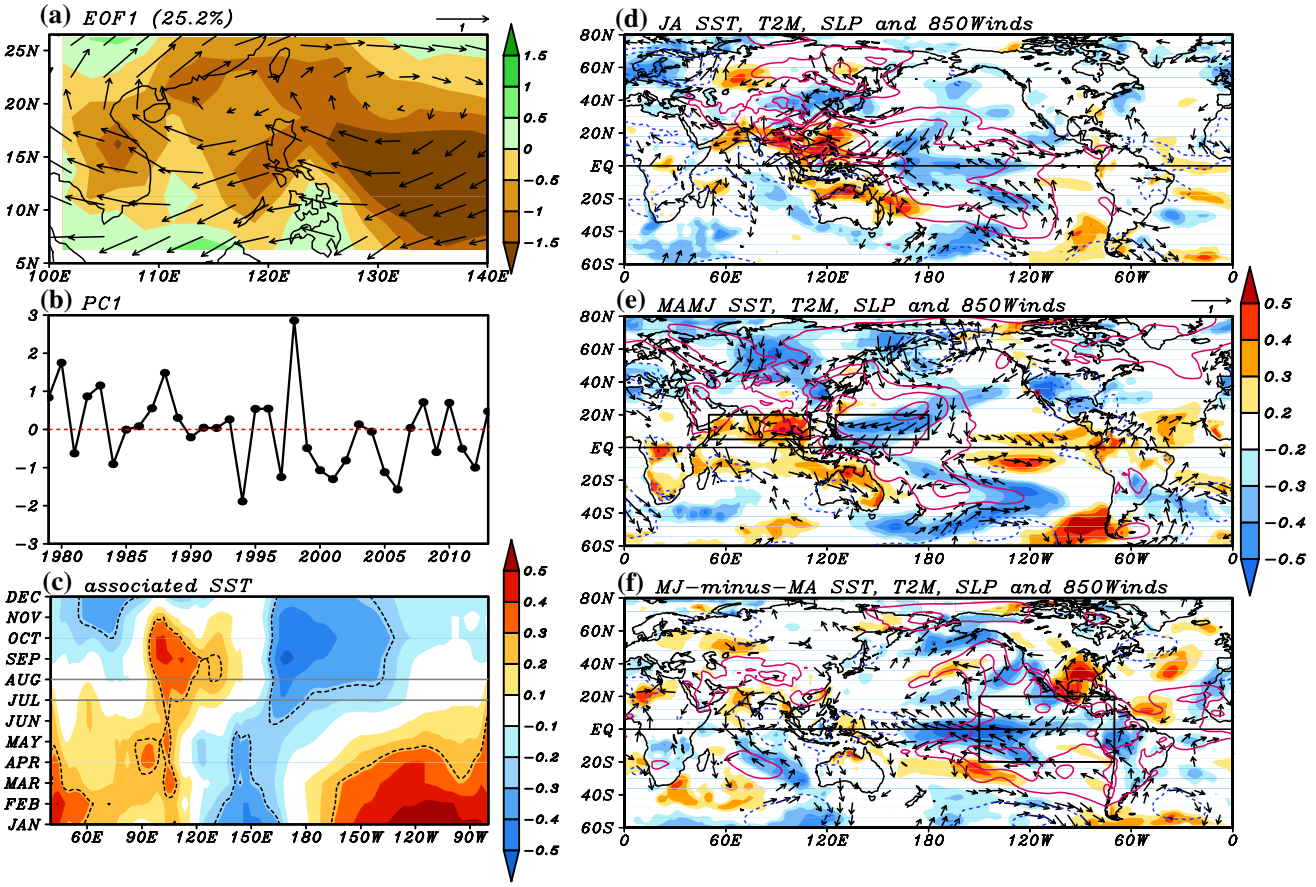

Fig. 3 **a** The spatial pattern and **b** the corresponding principal component of the first EOF mode (SEA-1) derived from JA precipitation over SEA for the period of 1979–2013. The simultaneous correlation coefficients of JA mean 850 hPa winds are also shown in Fig. 3a (*vectors*). **c** The lead-lag correlation map between the PC1 and the monthly mean SSTA averaged between 10°S and 10°N. The contour represents the correlation coefficient significant at the 90 % confidence level. **d** The simultaneous correlation map (with reference to the PC1) of the anomalous JA mean SST (*color shading* over ocean), 2 m air temperature (T2M, *color shading* over land), SLP (*contours*) and 850 hPa winds (*vectors*). **e**, **f** The same as in **d** except for the March through June mean (MAMJ), and May–June (MJ)-minus-March–April (MA), respectively. The *red solid contours* indicate positive correlation coefficient between SLP and PC1 starting from 0.2 with an interval of 0.2. Similar interval applies to *blue dashed* line but for negative correlation. The *rectangular* regions in Fig. 3e, f outline the area where the predictors are defined

from observational point of view. The first four modes can explain about 56 % of the total variance. For convenience of discussion, we will refer to the first EOF mode as SEA-1. Similar abbreviations apply to SEA-2, SEA-3, and SEA-4.

To detect the primary large scale drivers for each mode, we make correlation maps between surface temperature (ST) anomalies (the SST anomalies (SSTA) over ocean and 2 m air temperature (T2M) anomalies over land) and sea-level pressure (SLP) with reference to each PC. Stepwise multi-linear regression is used to establish the P-E model for each PC. Prior to the regression, all variables are normalized by removing their means and divided by their corresponding standard deviation. A detailed account of the PMA procedure and derivation of the P-E models are referred to Yim et al. (2004). In order to test the predictive capability of the P-E models for each PC, we systematically leave 3 years out from the period 1979–2013, then train the model using data of the remaining years and finally apply the model to forecast the three target years.

3 Origins of the major modes of SEA rainfall in the peak summer

The physical meaning of the four EOF modes and how they link to lower boundary anomalies will be discussed in this section. These EOF patterns and the corresponding PCs are shown in panels (a) and (b) of Fig. 3 through Fig. 6, respectively. The panels (c) in Fig. 3 through Fig. 6 present the relationship between each PC and the evolution

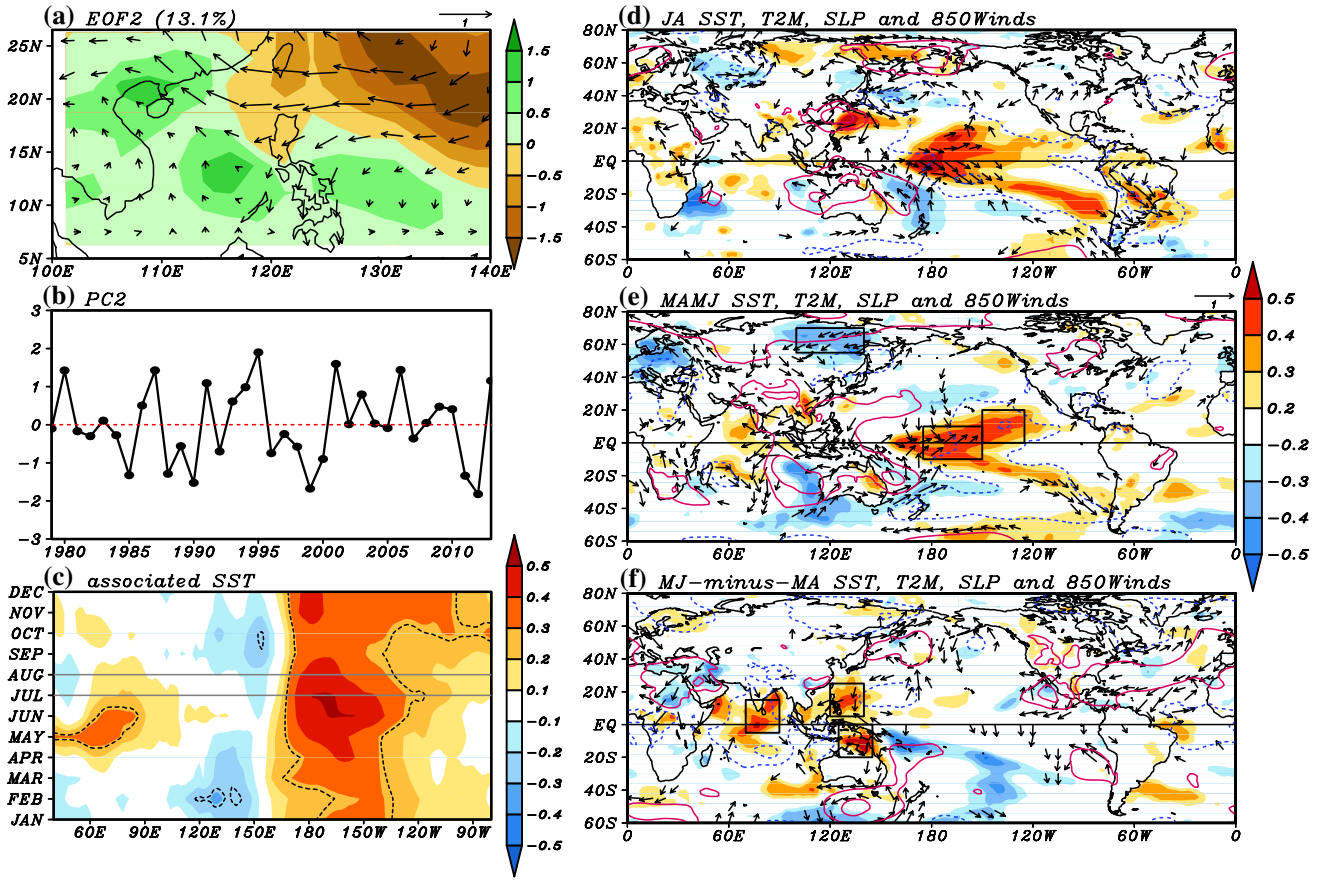

Fig. 4 Same as in Fig. 3 except for SEA-2

of the SST in the equatorial Indo-Pacific. The panels (d) in Fig. 3 through Fig. 6 show the simultaneous correlation maps between each PC and boundary layer anomalies and 850 hPa wind anomalies. The panels (e) and (f) in Figs. 3, 4, 5 and 6 display correlation maps of MAMJ mean and MJ-minus-MA ST/SLP anomalies with reference to each PC for seeking persistent and tendency predictors.

3.1 SEA-1: WPSH-dipole SST feedback mode in Northern Indo-western Pacific warm pool

The leading EOF mode (SEA-1) accounts for 27.4 % of the total precipitation variance. The spatial pattern shows a domain-wise uniform negative precipitation anomalies with a strong center over the Philippine Sea (Fig. 3a). This mode represents a pronounced weakening of the SEA tropical monsoon trough.

The monthly lead-lag correlation map of SEA-1 with the equatorial Indian-Pacific (40°E–80°W) SSTA averaged between 10°S and 10°N (Fig. 3c) shows that a prominent eastern Pacific (EP) warming appears during the previous winter and then rapidly decays from January to May followed by an onset of a subsequent cold event in the central Pacific (CP). Thus, a weakened SEA monsoon is associated with a rapid transition from a decaying EP El Niño to a developing CP La Niña, such as 1983, 1988, 1998, and 2008 (Fig. 3b). Conversely, during the developing CP warming in 1994, 1997, 2002 and 2006, the SEA monsoon is strengthened (Fig. 3b).

The correlation map between SEA-1 and 850 hPa wind anomaly from March to August (Fig. 3d, e) shows that an anomalous anticyclone persists from spring through the ensuring summer. This is consistent with the finding of Wang and Zhang (2002). Wang et al. (2000) attributed the persistence of the Philippine Sea anticyclone from previous winter to summer to a positive thermodynamic feedback between atmospheric descending Rossby waves and the underlying cold SST anomaly and suppressed convection to the southeast of the anticyclone center as can be seen from Fig. 3d, e. This anticyclone strengthens the WPSH in peak summer (Fig. 3d), accompanied by suppressed precipitation over the Philippine Sea and its neighborhood, suppressing the monsoon trough over the Philippine Sea. Note that the strengthening of the WPSH is concurrent with the development of the equatorial CP cooling (Fig. 3d), which contributes to enhancement of the WPSH by stimulating

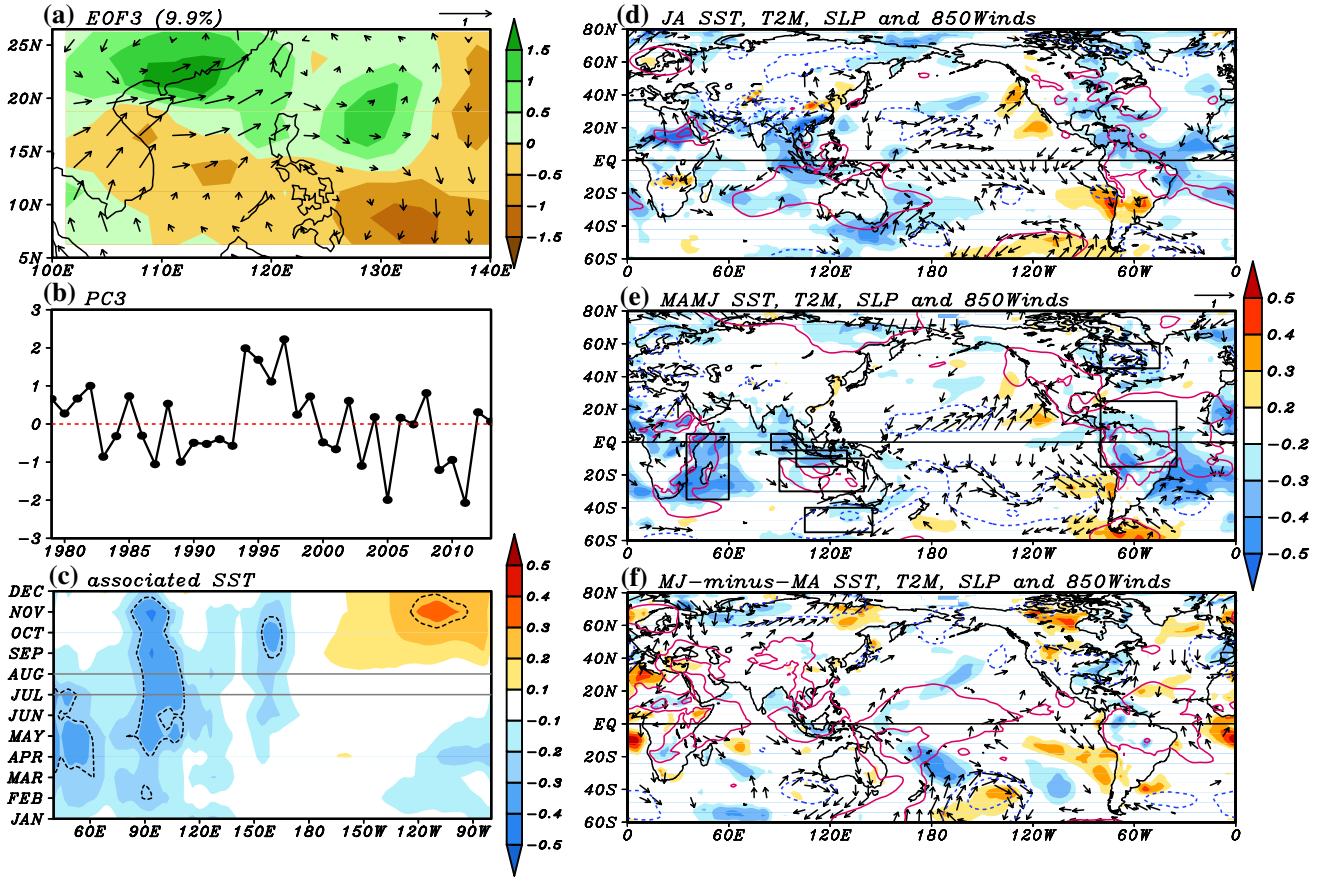

Fig. 5 Same as in Fig. 3 except for SEA-3

westward propagation descending Rossby waves. This air-sea interaction process has been confirmed by numerical experiments (e.g., Lau et al. 2004; Xiang et al. 2013).

In summary, the suppressed SEA rainfall is associated with a rapid transition from decaying EP El Niño to developing CP La Niña, whereas enhanced SEA rainfall is associated with a rapid transition from an EP La Niña to a CP El Niño. This transition is characterized and facilitated by a positive thermodynamic feedback between the WPSH and the underlying SST dipole: cooling to the southeast of the western North Pacific (WNP) anticyclonic anomaly and warming over the north Indian Ocean (IO, to the southwest of the WNP anticyclonic anomalies). The dipole SST anomaly results from the atmospheric forcing of the anomalous WPSH. The anomalous WPSH cools WNP because the anomalous northeasterly winds strengthen mean easterlies and warms the northern IO due to the extended anticyclone reducing the total wind speed and cloudiness. On the other hand, the western Pacific cooling suppresses convective heating, subsequently strengthening the WPSH. The northern IO warming is also indirectly favored of enhancing the WPSH (Wang et al. 2013; Xiang et al. 2013).

Based on our understanding of the physical process that determines the SEA-1 mode, we establish two predictors for prediction of the PC1. One is the persistent dipole differential SST anomalies during spring through early summer (MAMJ) between the northern IO (50°E–110°E, 5°N–20°N) and the WNP (125°E–180, 5°N–20°N), which is called MAMJ IO-WNP ST. This predictor reflects the warm pool atmosphere–ocean interaction that maintains the WNPSH anomalies. The other is SLP tendency anomalies from spring [March–April (MA)] to early summer (MJ) over tropical EP (150°W–70°W, 20°S–20°N) called MJ-MA EP SLP. This predictor signifies the development of equatorial easterly anomalies in the central Pacific, which leads to a rapid transition of ENSO cycle from EP warming to CP cooling or vice versa. These two predictors are physically more independent and their combination yields excellent simulation skill (r = 0.78).

3.2 SEA-2: Central Pacific (CP)-ENSO mode

SEA-2, which accounts for 13.1 % of the total variance, is characterized by a sharp contrast between prominent suppressed rainfall to the east of Taiwan and enhanced rainfall

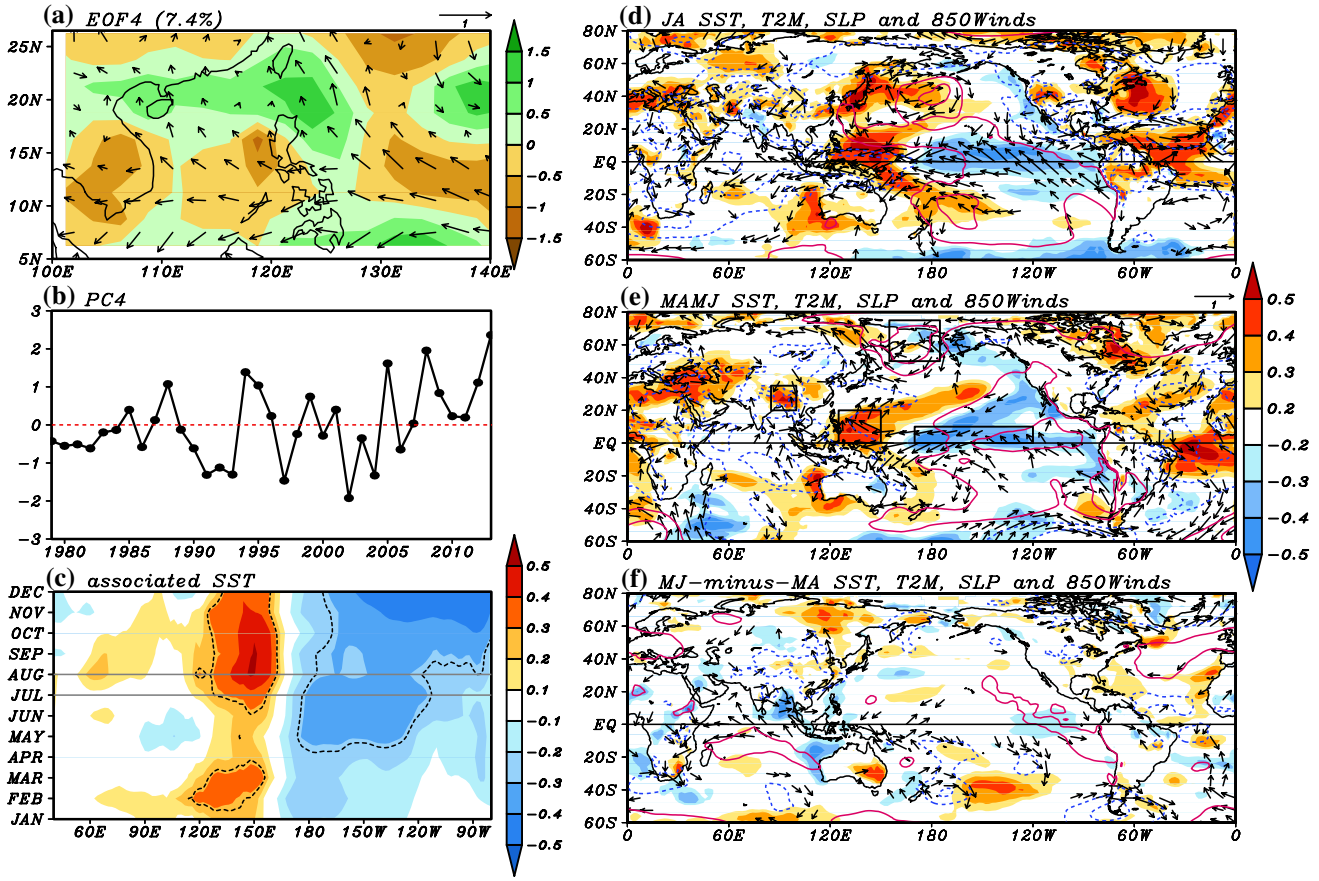

Fig. 6 Same as in Fig. 3 except for SEA-4

over the most southern part of China, Indo-China Peninsula, SCS and Philippine Sea (Fig. 4a). The reduced rainfall is caused by a local anomalous high SLP (Fig. 4d). The southern flank of the anomalous anticyclone transports abundant moisture, leading to enhanced rainfall to the south and southwest of the anticyclone (Fig. 4a). The corresponding PC2 shows an irregular year-to-year fluctuation (Fig. 4b).

The equatorial SSTA over western Indo-Pacific region associated with this mode show a long-lasting equatorial CP warming throughout the year with a maximum warming appearing in early summer (Fig. 4c). The precipitation pattern associated with SEA-2 is mainly influenced by the CP warming (Fig. 4d). Note that the CP warming here resembles the location of CP-ENSO (Kao and Yu 2009). Thus, this mode is called CP-ENSO mode, although CP-ENSO tends to mature in winter but here the warming peaks in boreal summer.

Affected by the CP warming, the rising branch of Walker circulation shifts eastward, weakening the convection activities over the tropical WP. The suppressed convective precipitation (not shown) can generate anomalous anticyclones to its west on both sides of the equator (Fig. 4e). On one hand, the anomalous anticyclone warms tropical WP SST through suppressing rainfall and increasing downward solar radiation. On the other hand, the tropical IO is also heated because the extended easterly associated with the anomalous anticyclones reduces the total wind speed during early summer. In this process, the MAMJ mean warming signals over tropical CP (175°E–150°W, 10°S–10°N and 150°W–125°W, 0–20°N, named MAMJ CP ST) (Fig. 4e) and the warming tendency over tropical WP (120°E–140°E, 5°N–25°N, and 125°E–145°E, 20°S–0) and IO (70°E–90°E, 5°S–15°N), called MJ-MA IO-WP ST) (Fig. 4f) are selected as two predictors. They are both important precursors for the high pressure anomaly to the east of Taiwan which directly impact the rainfall pattern of SEA-2.

It should be noticed that the lower T2M over the northern Eurasia is also a significant persistent signal. This might be linked to positive snow cover anomaly to certain extent. It has been recognized that the Eurasian snow cover anomaly in spring is one of the important factors affecting EA rainfall through a Eurasian wave train (Yim et al. 2010). Thus, the persistent T2M anomalies over the northeastern Eurasia (100°E–140°E, 55°N–70°N), which is defined as

MAMJ NEU ST (Fig. 4e), is selected as the third predictor for SEA-2.

3.3 SEA-3: Maritime continent SST-Australian High coupled mode

Figure 5a shows the spatial pattern of SEA-3 which accounts for nearly 10 % of total variance. The SEA-3 mode features a rainfall anomaly center over southern China near Guangdong Province, expanding to the northern Philippine Sea, while suppressed rainfall occurs to the south of the enhanced rainfall belt. This anomalous rainfall pattern is associated with a low pressure anomaly in southern China and an anomalous anticyclonic circulation centered over the southern SCS and connected with a cross-equatorial flow and enhanced Australian anticyclone (Fig. 5d). The SCS anticyclone is the major circulation system (Fig. 5a) that caused the SEA-3 rainfall anomaly pattern. A notable anomalous southerly and southwesterly flow runs along the western and northwestern edge of the anomalous southern SCS High. The corresponding PC shows decadal change with a positive phase during mid-1990s and a negative phase before 1990s and after 2000s (Fig. 5b).

Different from SEA-1 and SEA-2 which have a clear relationship with SSTA over CP and EP areas, the PC3 has no significant correlation with ENSO. The SEA-3, however, is preceded and concurs with a cooling over the Maritime continent (MC) and eastern IO (Fig. 5c).

The MC cooling suppresses precipitation over the MC, hence enhances the South China Sea anticyclone by exciting descending Rossby wave north of the equator. For this reason, we picked up the persistent predictor MAMJ MC ST (Fig. 5e) to foreshadow the MC SST cooling. This predictor is defined by MAMJ mean SSTA averaged over domain A (35°E–60°E, 35°S–5°N), domain B (85°E–100°E, 5°S–5°N) and domain C (100°E–130°E, 15°S–5°S) (Fig. 5e). The definition includes a western Indian Ocean (domain A) cooling, but the domain A cooling is not essential. If we exclude the WIO cooling in this predictor, the overall skills for the SEA region (shown later) are unchanged. For this reason, we named this predictor as MAMJ MC ST.

Why can the MC SST cooling persist from MAMJ (the austral fall to early winter) to JA (the peak austral winter)? We argue that this persistent cooling is a result of a positive feedback between the anomalous Australian High and the adjacent ocean over the MC. The positive feedback process between a Southern Hemisphere anomalous anticyclone and adjacent ocean has been discussed by Wang et al. (2003). Here, an enhanced Australian anticyclone can advect cold air from midlatitude to the sea surfaces over the MC and the anomalous southeast wind off-coast of Sumatra can induce anomalous upwelling, both contribute to the cooling over the sea surface of the MC. On the other hand, the cooling sea surface suppresses MC convection that in turn enhances the Australian High by inducing a descending Rossby wave response in the Southern Hemisphere. For this reason, the anomalous Australian High in MAMJ is also chosen as a predictor. This predictor is called MAMJ AH SLP and is defined by the SLP anomalies averaged over (90°E–140°E, 30°S–10°S) minus (105°E–145°E, 55°S–40°S) (Fig. 5e).

In addition to the signals from southern hemisphere, the SEA-3 is also linked to the SLP anomalies over North Atlantic which is associated with a positive NAO. Previous study suggested that anomalous NAO in spring (April–May) can induce a tripole SST pattern in North Atlantic that excites a teleconnection pattern across Eurasia and consequently influence EASM rainfall (Wu et al. 2009, Yim et al. 2013). Therefore, the MAMJ mean SLP dipole over North Atlantic can be a potential predictor. The predictor MAMJ NA SLP is defined by the SLP anomalies averaged over (80°W–35°W, 15°S–25°N) minus (80°W–45°W, 45°N–60°N).

3.4 SEA-4: ENSO developing mode

The fourth mode accounts for 7.4 % of the total variance. The distribution of rainfall anomaly seems more complicated and irregular than the first three modes (Fig. 6a). Generally, it exhibits a south-north contrasting pattern with suppressed rainfall band along 5°N–15°N while enhanced rainfall between 15°N and 25°N. The formation of such pattern is affected by the anomalous easterly south of 15°N, which signifies the weakening of the tropical monsoon. Besides interannual variation, the corresponding PC also shows increased trend within the 35 years especially after 2000 (Fig. 6b).

The relationship of SEA-4 with equatorial SST anomalies is illustrated in Fig. 6c. There is a significant contrast between warming SSTA over WP warm pool region and cooling anomalies along tropical central and eastern Pacific (CEP). The negative SSTA becomes wider and stronger gradually and peaks in the following winter over EP. Thus, this mode is called ENSO developing mode.

The different SSTA between WP and CEP and the associated anomalous walker circulation can be captured in Fig. 6d, e. As shown in the two panels, the enhanced trade winds in the equatorial Pacific is consistent with anomalous cooling (warming) in the EP (WP). The increased SST gradient strengthens easterly anomaly which suppresses rainfall over Indo-China peninsula, southern SCS and Philippine Sea as shown in Fig. 6a due to the weakened monsoon trough. The different SSTA over WP (125°E–150°E, 0–20°N) and CEP (170°E–120°W, 0–10°N) during MAMJ is an important precursor for SEA-4 and is selected as one predictor named MAMJ WP-EP ST (Fig. 6e).

Table 1 Definition of each predictor selected for the prediction of each PC and the corresponding prediction equation

PC	Name	Definition	Prediction equation
SEA-1	MAMJ IO-WNP ST	MAMJ ST (50°E–100°E, 5°N–20°N) − (125°E–180, 5°N–20°N)	0.4825*MAMJ IO-WNP ST + 0.4977*MJ-MA EP SLP
	MJ-MA EP SLP	MJ-minus-MA SLP (150°W–70°W, 20°S–20°N)	
SEA-2	MAMJ CP ST	MAMJ ST (175°E–150°W, 10°S–10°N) + (150°W–125°W, 0–20°N)	0.2366*MAMJ CP ST − 0.2649*MAMJ NEU ST + 0.4581*MJ-MA IO-WP ST
	MAMJ NEU ST	MAMJ ST (100°E–140°E, 55°N–70°N)	
	MJ-MA IO-WP ST	MJ-minus-MA ST (120°E–140°E, 5°N–25°N) + (125°E–145°E, 20°S–0) + (70°E–90°E, 5°S–15°N)	
SEA-3	MAMJ MC ST	MAMJ ST (35°E–60°E, 35°S–5°N) + (85°E–100°E, 5°S–5°N) + (100°E–130°E, 15°S–5°S)	−0.3630*MAMJ MC ST + 0.2410*MAMJ AH SLP + 0.3311* MAMJ NA SLP
	MAMJ AH SLP	MAMJ SLP (90°E–140°E, 30°S–10°S) − (105°E–145°E, 55°S–40°S)	
	MAMJ NA SLP	MAMJ SLP (80°W–35°W, 15°S–25°N) + (80°W–45°W, 45°N–60°N)	
SEA-4	MAMJ WP-EP ST	MAMJ ST (125°E–150°E, 0–20°N) − (170°E–120°W, 0–10°N)	0.2575*MAMJ WP-EP ST + 0.2881* MAMJ TP ST + 0.3917* MAMJ NP SLP
	MAMJ TP ST	MAMJ ST (85°E–100°E, 20°N–35°N)	
	MAMJ NP SLP	MAMJ SLP (155°E–175°W, 50°N–75°N)	

A persistent T2M positive anomaly, which can be seen clearly over the eastern Tibetan Plateau (TP, 85°E–100°E, 20°N–35°N, Fig. 6e), is also selected as one predictor. It has been pointed out by Wang et al. (2008) that atmospheric heating induced by the rising TP temperatures may deform the WPSH and enhances moisture convergence toward the EA subtropical front, which leads to anomalous summer frontal rainfall in EA region. This predictor is called MAMJ TP ST. The third precursor of the SEA-4 is the persistent weakening of Aleutian low (Fig. 6e). It leads to an anomalous anticyclone in the northwestern Pacific (Fig. 6d), which seem to affect northern EA but could also contribute to the SEA rainfall anomalies. To depict the anomalous SLP over and to the north of the Aleutian Low, a predictor MAMJ NP SLP is defined by the SLP anomalous averaged over (155°E–175°W, 50°N–75°N).

4 Estimated predictability and prediction with P-E models

4.1 Prediction of each PC

In order to make JA rainfall prediction over SEA, a set of P-E models is established through stepwise multi-linear regression method using the predictors introduced in Sect. 3. The idea is to first predict each PC and then use observed EOF pattern and the corresponding predicted PC to make a rainfall prediction at each grid point.

The precise definition of the predictors for each PC and the corresponding equations are presented in Table 1. All these predictors are selected by stepwise regression given the F-test at 90 % confidence level. In our case, EOF analysis is performed using the data during 1979–2013. The cross-validation method (Michelson 1987) is used to make a retrospective forecast for each PC. To lessen over-fitting problem, we leave 3 years of data out progressively centered on a forecast target year for the period 1979–2013, then train the model using data of the remaining years and finally apply the model to forecast the three target years. The predicted PCs using the set of P-E models (P-EM) in the cross-validated mode are shown by the red line in Fig. 7a–d compared with the corresponding observed PCs (black line in each panel). The cross-validated correlation skill between observation and prediction is 0.72, 0.64, 0.52, and 0.61 for the first four PCs, respectively. Note also the simulated correlation skills are higher than the cross-validation, which are 0.78, 0.69, 0.67 and 0.69 for the first four PCs, respectively. The correlation coefficients are all significant at 99 % level, which means that, to a large extent, the first four modes can be regarded as predictable mode.

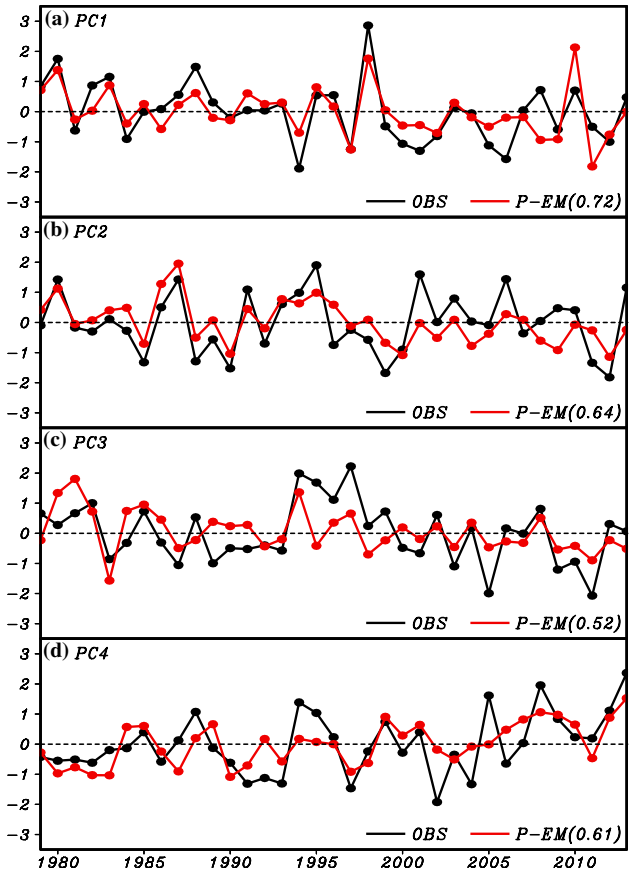

Fig. 7 The corresponding PCs of the first four EOF modes in observation (OBS, *black line*) and cross-validated prediction model (P-EM) from 1979 to 2013. The cross-validation was done by taking 3-year out around the predicted year. The numbers within the parenthesis in the figure legend indicate the correlation coefficient between the observed and predicted PC

4.2 Prediction of peak-summer precipitation over SEA

Based on the predicted PC1 through PC4 in Sect. 4.1, we can predict precipitation anomalies over SEA using the sum of the observed four spatial patterns (SEA1 through SEA4) multiplied by the corresponding predicted PCs. It should be noted that all predictors can be obtained 5-day before July1 because the values for the last 5 day can be obtained from weather forecast, so the prediction here is a 0-month lead prediction.

The spatial distribution of the TCC skill is given in Fig. 8b. The domain-averaged TCC skill is 0.44. The land rainfall prediction skill containing southern China, Indo-China peninsula and Philippine is 0.35. Significant high skill is found over several climatological rainfall centers. The skill is limited over eastern coast of Indo-China peninsula and the western SCS where the climatological mean precipitation rate in much less than other regions (Fig. 2).

The red line in Fig. 8c shows the time series of spatial pattern correlation (PCC) skill for each year between observed precipitation anomalies and predicted field. The PCC skill shows large year-to-year variation. The 35-year mean PCC skill is 0.42. There are 9 years with high skill (above 0.6) and 7 years with low skill (below 0.2).

4.3 Potential predictability

As discussed before, the first four modes are considered to be predictable. In this subsection, we compute the potential attainable forecast skill for peak-summer precipitation over SEA. The observed predictable part is reconstructed by the linear combination of the first four modes. Supposing that these modes can be predicted perfectly, the potentially maximum attainable forecast skill can be estimated from the correlation between the observed precipitation anomaly and the reconstructed predictable part of the rainfall using the four predictable modes.

The maximum attainable TCC skill estimated by the first four modes is shown in Fig. 8a. The domain-averaged correlation skill is 0.68. High predictability regions locate over Indo-China peninsula, southern coast of China, southeastern SCS, and Philippine Sea with the TCC higher than 0.8 (Fig. 8a). These regions are consistent with rainfall centers shown in the climatology map in Fig. 2. The maximum attainable anomalous pattern correlation coefficient (PCC) skill for each forecast year is shown by the black line in Fig. 8c. The 35-year mean PCC is 0.67. There is large year-to-year variation in the maximum attainable skill between 0.4 and 0.9. There are 8 years during which the maximum attainable PCC skill is above 0.8 (1980, 1983, 1994, 1995, 1997, 1998, 2005 and 2006). The year of 2007 is exceptionally low (below 0.4). Among the 7 years with low prediction skill, the skills in 1984, 1989, 1996, and 2007 are particularly low (red line in Fig. 8c). These years are La Niña years and the potential predictability are not particularly low (except 2007), suggesting that the P-E models have deficiencies in capturing La Niña impacts.

5 Summary

The present study investigates the peak summer (JA) seasonal rainfall predictability and prediction over the tropical EA or Southeast Asia (SEA) for the 35-year period of 1979–2013.

The first four major modes of SEA rainfall variability are identified using PMA, which explains about 56 % of the total observed variability. We provided physical interpretations to each of them. The physical processes that affect each mode is different and can be summarized as follows: (1) the SEA-1 often occurs during rapid ENSO

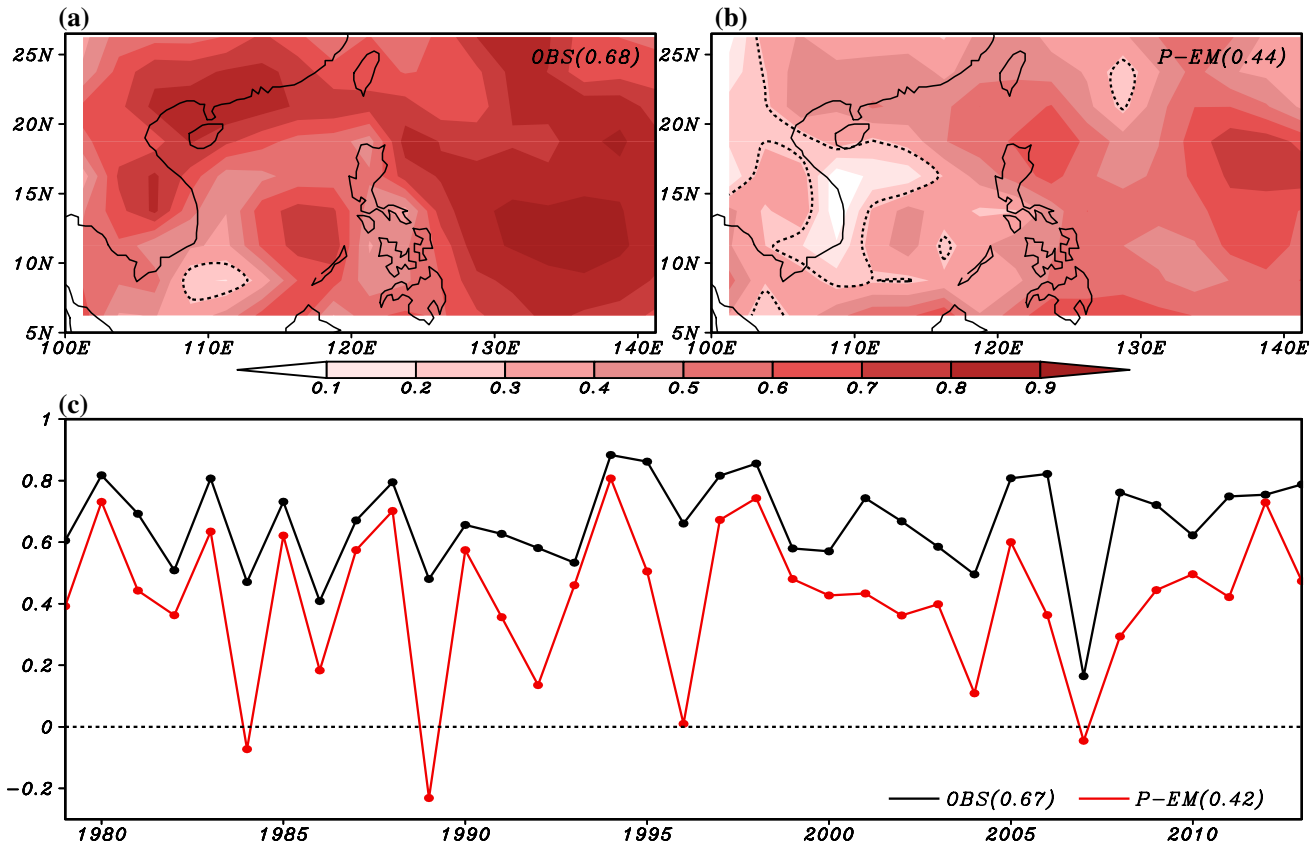

Fig. 8 The temporal correlation coefficient (TCC) skill for JA precipitation prediction over SEA by using the **a** observed first four modes (OBS), **b** the P-E Models. The *dashed contour* is the TCC skill of 0.28 which is statistically significant at 90 % confidence level. The numbers within the parenthesis in right corner of each figure indicate the domain-averaged TCC skill. **c** The pattern correlation coefficient (PCC) skill for JA precipitation prediction over SEA as a function of forecast year using the 3-year out cross-validated P-E model prediction (*red line*). The potential attainable forecast skill obtained by using observed four PCs (OBS, *black line*) is also compared. The numbers within the parenthesis in the figure legend indicate the averaged PCC skill through the 35 years

decay-transition and is caused by a positive feedback between the western Pacific subtropical high (WPSH) anomaly and underlying warm pool SST dipole, (2) the SEA-2 is primarily induced by the persist anomalous equatorial central Pacific SST, (3) the SEA-3 is caused mainly by the interaction between anomalous Australian High and SSTA over MC, and (4) SEA-4 is associated with EP-ENSO development.

These findings provide dynamical insights into the physical processes that control the JA precipitation variability over SEA, and may have important implications for better prediction. To make a seasonal prediction and to estimate potential predictability, a set of 0-month lead P-E models is established for prediction of first four leading PCs. All the predictors are selected based on either persistent atmospheric lower boundary anomalies during spring through early summer or the tendency from spring to early summer. Emphasis is put on physical understanding the lead-lag relationship between the predictors and predictand. Only two to three predictors are used for each PC. The cross-validated TCC skill for prediction of each PC is between 0.52 and 0.72 which are all significant at 99 % level. Thus, to a large extent, the first four modes can be regarded as predictable mode, at least in terms of the P-E model estimation.

The cross-validated hindcast skill using P-E model (domain-averaged TCC skill r = 0.44, Fig. 8b) is twice higher than the skill of the current dynamical models' multi-model ensemble hindcast skill (r = 0.19, Fig. 1). The P-E model's prediction sets up a benchmark for dynamic climate models. The results here suggest that the current dynamical models have large rooms to improve.

The predictability for JA rainfall over SEA is also discussed using these predictable modes (Fig. 8). Almost the whole domain has significantly high predictability (as measured by the maximum attainable correlation skill), especially over the Indo-China peninsula, the southern coast of China, the southeastern SCS, and Philippine Sea where with the climatological rainfall centers are located (Fig. 2).

Most of the PC predictors are related to tropical SST anomalies or atmosphere–ocean interaction, suggesting that the main sources of predictability of the JA SEA rainfall are rooted in tropics. However, there are some minor predictors reflect land surface or extratropical anomalous conditions, such as the northeastern Eurasian surface air temperature (for SEA-2), the North Atlantic and southern hemisphere SLP (for SEA-3), and Tibetan plateau warming and Aleutian SLP (for SEA-4). The linkages between these extratropical predictors and the corresponding PCs are not completely understood and our explanations need more rigorous justifications.

It should be noted that most predictable modes are associated with observed SSTA over equatorial CP and EP except for SEA-3, which accounts for almost 10 % of the total variance (Fig. 5c). Understanding the physical process and variability sources of this non-ENSO-related mode is necessary, especially during ENSO neutral years when it may become major sources of rainfall variability during peak summer (Wang et al. 2009). However, the TCC for SEA-3 between prediction and observation is lower than the other three modes. Better understanding of this mode is still needed to improve the forecast skill of this mode.

In order to improve the prediction skill using dynamical model, a dynamical-statistical method can be introduced using the output of lower boundary anomalies and anomalous large scale circulation derived from the dynamical prediction as predictors. Whether this will be better than the models' direct prediction of the rainfall will be further studied.

Acknowledgments This work was jointly supported by APEC climate center (APCC), the National Research Foundation (NRF) of Korea through a Global Research Laboratory (GRL) grant of the Korean Ministry of Education, Science and Technology (MEST, #2011-0021927) and NSFC-Shandong Joint Fund for Marine Science Research Centers (Grant No. U1406401). We also acknowledge support from China Scholarship Council (CSC) and the International Pacific Research Center (IPRC). This is publication No. 9229 of the SOEST, publication No. 1091 of IPRC and publication No. 20 of Earth System Modeling Center (ESMC).

References

Chang CP, Zhang Y, Li T (2000) Interannual and interdecadal variations of the East Asian summer monsoon and tropical Pacific SSTs. Part I: roles of the subtropical ridge. J Clim 13:4310–4325

Chen TJG, Chang CP (1980) The structure and vorticity budget of an early summer monsoon trough (Mei–Yu) over southeastern China and Japan. Mon Wea Rev 108:942–953

Dee DP et al (2011) The ERA-interim reanalysis: configuration and performance of the data assimilation system. Q J R Meteorol Soc 137:553–597

Delworth TL, Broccoli AJ, Rosati A et al (2006) GFDL's CM2 global coupled climate models. Part I: formulation and simulation characteristics. J Clim 19:643–674

Ding YH (1992) Summer monsoon rainfalls in China. J Meteor Soc Jpn 70:397–421

Ding YH, Chan JCL (2005) The East Asian summer monsoon: an overview. Meteorol Atmos Phys 89:117–142

Fan K, Liu Y, Chen HP (2012) Improving the prediction of the East Asian summer monsoon: new approaches. Weather Forecast 27(4):1017–1030

He JH, Wu ZW, Jiang ZH, Miao CS, Han GR (2007) "Climate effect" of the northeast cold vortex and its influences on Meiyu. Chin Sci Bull 52(5):671–679

Hudson D, Alves O, Hendon HH, Wang G (2010) The impact of atmospheric initialisation on seasonal prediction of tropical Pacific SST. Clim Dyn 36:1155–1171

Huffman GJ, Bolvin DT, Adler RF (2011) Last updated GPCP Version 2.2 combined precipitation data set. WDC-A, NCDC, Asheville, NC (2011). Dataset Accessed at http://www.ncdc.noaa.gov/oa/wmo/wdcamet-ncdc.html

Kao HY, Yu JY (2009) Contrasting eastern-Pacific and central Pacific types of El Niño. J Clim 22:615–632

Kosaka Y, Yang S (1997) Climatology and interannual variability of the Southeast Asian summer monsoon. Adv in Atmos. Sci. 14(2):141–162

Lau KM, Yang GJ, Shen H (1988) Seasonal and intraseasonal climatology of summer monsoon rainfall over East Asia. Mon Wea Rev 116(1):18–37

Lau NC, Nath MJ, Wang H (2004) Simulations by a GFDL GCM of ENSO-related variability of the coupled atmosphere-ocean system in the East Asian monsoon region. In: Chang CP (ed) East Asian monsoon, World Scientific series on meteorology of East Asia No. 2. World Scientific, Singapore, pp 271–300

Li B, Zhou T (2011) ENSO-related principal interannual variability modes of early and late summer rainfall over East Asia in SST-driven AGCM simulations. J Geophys Res 116(D14118): 1–15

LinHo Wang B (2002) The time-space structure of the Asian-Pacific summer monsoon: a fast annual cycle view. J Clim 15:164301658

Liu X, Yanai M (2002) Influence of Eurasian spring snow cover on Asian summer rainfall. Int J Climatol 22(9):1075–1089

Luo JJ, Masson S, Behera S, Shingu S, Yamagata T (2005) Seasonal climate predictability in a coupled OAGCM using a different approach for ensemble forecast. J Clim 18:4474–4497

Michaelsen J (1987) Cross-validation in statistical climate forecast model. J Clim Appl Meteorol 26:1589–1600

Qin S, Riyu L, Chaofan L (2013) Large-scale circulation anomalies associated with interannual variation in monthly rainfall over South China from May to August. Adv Atmos Sci. doi:10.1007/s00376-013-3051-x

Saha S et al (2013) The NCEP climate forecast system version 2. J Clim, Accepted

Smith TM, Reynolds RW, Peterson TC, Lawrimore J (2008) Improvements to NOAA's historical merged land-ocean surface temperature analysis (1880–2006). J Clim 21:2283–2296

Tao S, Chen L (1987) A review of recent research on the East Asian summer monsoon in China. In: Chang CP, Krisnamurti TN (eds) Monsoon meteorology. Oxford University Press, Oxford, pp 60–92

Wang B, LinHo YS (2002) Rainy seasons of the Asian-Pacific monsoon. J Clim 15:386–398

Wang B, Zhang Q (2002) Pacific-East Asian teleconnection, part II: How the Philippine Sea anticyclone established during development of El Nino. J Clim 15:3252–3265

Wang B, Wu R, Fu X (2000) Pacific-East Asia teleconnection: How does ENSO affect East Asian climate? J Clim 13:1517–1536

Wang B, Wu R, Lau KM (2001) Interannual variability of the Asian Summer Monsoon: contrasts between the Indian and the Western North Pacific-East Asian Monsoons. J Clim 14(20):4073–4090

Wang B, Wu R, Li T (2003) Atmosphere-Warm ocean interaction and its impact on Asian-Australian monsoon variation. J Clim 16:1195–1211

Wang B, Ding Q, Fu X, Kang IS, Jin K, Shukla J, Doblas-Reyes F (2005) Fundamental challenge in simulation and prediction of summer monsoon rainfall. Geophys Res Lett 32(15):L15711. doi:10.1029/2005GL022734

Wang B, Lee JY, Kang IS, Shukla J, Hameed SN, Park CK (2007) Coupled predictability of seasonal tropical precipitation. CLIVAR Exchanges 12:17–18

Wang B, Bao Q, Hoskins B, Wu G, Liu Y (2008) Tibetan Plateau warming and precipitation change in East Asia. Geophys Res Let 35:L14702. doi:10.1029/2008GL034330

Wang B, Liu J, Yang J, Zhou T, Wu Z (2009) Distinct principal modes of early and late summer rainfall anomalies in East Asia. J Clim 22:3864–3875

Wang B, Xiang B, Lee JY (2013) Subtropical high predictability establishes a promising way for monsoon and tropical storm predictions. PNAS 10:2718–2722

Wang B, Lee JY, Xiang B (2014) Asian summer monsoon rainfall predictability: a predictable mode analysis. Clim Dyn. doi:10.1007/s00382-014-2218-1

Wu Z, Li J (2008) Prediction of the Asian-Australian monsoon interannual variations with the grid-point atmospheric model of IAP LASG (GAMIL). Adv Atmos Sci 25(3):387–394

Wu Z, Wang B, Li J, Jin FF (2009) An empirical seasonal prediction of the east Asian summer monsoon using ENSO and NAO. J Geophys Res 114:D18120. doi:10.1029/2009JD011733

Xiang B, Wang B, Yu W, Xu S (2013) How can anomalous western North Pacific subtropical high intensify in late summer? Geophys Res Lett. doi:10.1002/grl.50431

Yim SY, Jhun JG, Lu R, Wang B (2010) Two distinct patterns of spring Eurasian snow cover anomaly and their impacts on the East Asian summer monsoon. J Geophys Res 115:D22113, pp 10. doi:10.1029/2010JD013996

Yim SY, Wang B, Kwon M (2013) Interdecadal change of the controlling mechanisms for East Asian early summer rainfall variation around the mid-1990s. Clim Dyn 1–9

Yim SY, Wang B, Xing W (2014) Prediction of early summer rainfall over South China by a physical-empirical model. Clim Dyn. doi:10.1007/s00382-013-2014-3

Zhang YS, Li T, Wang B (2004) Decadal change of the spring snow depth over the Tibetan Plateau: the associated circulation and influence on the east Asian summer monsoon. J Clim 17(14):2780–2793

Zhou TJ, Zou LW (2010) Understanding the predictability of East Asian Summer Monsoon from the reproduction of land-sea thermal contrast change in AMIP-Type simulation. J Clim 23(22):6009–6026

Zhu Q, He J, Wang P (1986) A study of circulation differences between East-Asian and Indian summer monsoons with their interaction. Adv Atmos Sci 3(4):466–477